Letter

Periodic driving shape controls energy transmission

Christian Simadji Ngamou,[1,*] Frank Thomas Ndjomatchoua,[2,†] and Clément Tchawoua[1,‡]

[1]*Laboratory of Mechanics and Complex Systems, Department of Physics, Faculty of Science, University of Yaoundé 1, P.O. Box 812, Ngoa Ekelle, Yaoundé, Cameroon*

[2]*Epidemiology and Modelling Group, Department of Plant Sciences, School of the Biological Sciences, University of Cambridge, Cambridge CB2 3EA, United Kingdom*

(Received 12 December 2023; accepted 25 April 2024; published 29 May 2024)

In the early 2000s, Geniet and Leon [Phys. Rev. Lett. **89**, 134102 (2002)] discovered the nonlinear supratransmission (NST) in a medium with a forbidden frequency band gap. It is a process in which nonlinear structures are created by a sinusoidal harmonic boundary condition imposed at a frequency in the band gap. The present study extends this concept and shows that an optimal shape of a periodic nonsinusoidal excitation may induce (or inhibit) energy flow through the lattice below (or above) the NST threshold, demonstrating that nonlinear supratransmission is reliant not only on the driving amplitude but also on its shape. This is evidenced through numerical simulations and mathematical calculations varying the excitation signal shape in the Fermi-Pasta-Ulam case study. Setting the shape parameter to zero recovers the results of the literature in relation to the sinusoidal signal.

DOI: 10.1103/PhysRevE.109.L052201

Introduction. A periodic boundary condition placed at a frequency in the band gap creates nonlinear structures termed gap solitons in a medium with a naturally forbidden frequency band gap (FFBG) [1]. The NST phenomenon is induced by an instability of the evanescent wave profile of the drive over a critical amplitude [2–4], and it may be found in a variety of physical systems, including mechanical [1], electrical [2], and optical arrays [5]. The system can be multicomponent [6], two-dimensional [7], diatomic [8], cross-linked [9,10], conical granular [11], or flat-band lattices [12].

The NST is controlled in unique circumstances such as inelastic impact limitations [13], collective escape [14], waves collisions [15], noise [16], impurity [17], finite-size effect [18], zero-frequency drive [10], disorder [19,20], or hysteretic damping [21]. The unanswered topic of how this phenomenon may develop from nonsinusoidal external signals motivated the present study.

Although harmonic sinusoidal driving is the most common kind of excitation in prior studies [1–21], it does not reflect generic excitations seen in nature and is mostly a solution of linear systems. Nonsinusoidal and shape-varying periodic forces driving nonlinear systems have lately attracted attention. A sole adjustment of the external driving force shape (with its period and amplitude kept constant) can regulate chaos, escape, and resonance, to name a few examples [22–24]. It can control the mobility and stability of intrinsic localized modes in nonlinear lattices [25,26].

While previous studies have all looked for a driving amplitude threshold greater than a certain value (frequency-dependent) known as the supratransmission threshold to trigger wave propagation [1–11,13–20], obvious questions arise, such as the following: *Can the NST phenomenon be controlled with signal parameters other than its amplitude?* The present study shows that a signal shape may induce (or inhibit) FFBG energy flow through the lattice, indicating that NST is dependent on signal form as well as driving amplitude.

Nonlinear Lattice and the External Signal. We consider the β-Fermi-Pasta-Ulam (FPU) system $\ddot{u}_n = u_{n-1} - 2u_n + u_{n+1} - (u_{n+1} - u_n)^3 + (u_n - u_{n-1})^3$, where $n = 1, 2, 3, \ldots, N-1, N$ [27]; u_n stands for the displacement from its equilibrium position of the nth particle of unit mass. This model is selected as an illustrative case study for the sake of simplicity and comparison purposes with literature results [27], but any other nonlinear lattice [1–21] can be analyzed, too. After setting the plane-wave solution $u_n(t) = A\cos(\omega t - qn)$, with q and ω the wave number and frequency, respectively, the linear dispersion relation is $\omega(q) = \sqrt{2[1-\cos(q)]}$. For q in the first Brillouin zone [28] ($q \in [0,\ \pi]$), the FFBG is $\omega \in]2, \infty[$. To study the effects of variable shape excitation, two types of boundary conditions

$$u_0(t) = \begin{cases} u_0^{(1)} = A\,\mathrm{sn}\left(\frac{2\kappa(r)\omega}{\pi}t\right), \\ u_0^{(2)} = A\frac{2r+(1+r^2)\cos(\omega t)}{1+r^2+2r\cos(\omega t)}, \end{cases} \tag{1}$$

are considered. In Eq. (1), $\mathrm{sn}(\bullet)$ is the Jacobi elliptic function and $\kappa(\bullet)$ is the complete elliptic function of the first kind. The variable r is the shape parameter of the time-periodic function $u_0(t)$ with the frequency ω. When the parameter r is varied (Fig. 1), the functions $u_0^{(1)}$ and $u_0^{(2)}$ keep the same amplitude A and period $T = 2\pi/\omega$ and adopt symmetric and asymmetric shapes, respectively. The functions $u_0^{(1)}$ (Jacobi elliptic) and $u_0^{(2)}$ (modified Remoissenet-Peyrard function) [22,23] are crafted in such a way that when $r = 0$, the usual harmonic

*Corresponding author: christthichi@gmail.com
†ftndjomatchoua@gmail.com/tfn21@cam.ac.uk
‡ctchawa@yahoo.fr

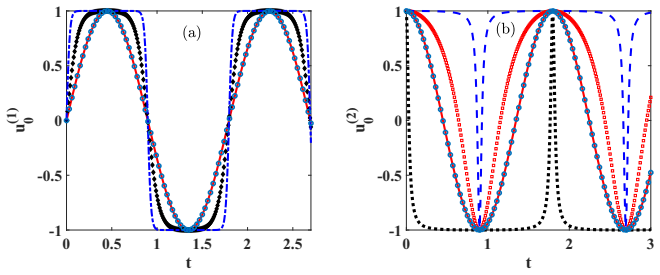

FIG. 1. Signals $u_0^{(1)}$ and u_0^2 for several values of the shape parameter r: (a) blue dash-dotted line ($r = 1$–10^{-10}), black diamond ($r = 0.99$), red solid line ($r = 0$). The blue circles stand for sinusoidal signal $A_0 \sin(\omega t)$; (b) black dotted line ($r = -0.9$), red solid line ($r = 0$), red squares ($r = 0.35$), blue dashed line ($r = 0.9$). Blue circles stand for the sinusoidal signal $A_0 \cos(\omega t)$. For both figures, the amplitude and the frequency are $A_0 = 1$ and $\omega = 3.5$, respectively.

functions $u_0(t) = A\sin(\omega t)$ and $u_0(t) = A\cos(\omega t)$ used in the NST literature [1–11,13–20] are recovered, respectively. Therefore, they represent generalized nonsinusoidal periodic functions.

Analytical Treatment of the NST. To gain a good understanding of the shape parameter effect, the methodology employed in Refs. [14,27,29] for estimating analytically the NST threshold is employed. Following Refs. [30,31], by using the Fourier series expansion of the function $u_0^{(1)}$, and keeping only the first three terms, the elliptic deformable function can be rewritten as a sum of sinusoidal signals

$$\frac{u_0^{(1)}(t)}{A} = \chi_1 \sin(\omega t) + \chi_3 \sin(3\omega t) + \chi_5 \sin(5\omega t), \qquad (2)$$

where $\chi_1 = \frac{2\pi}{r\kappa(r)} \frac{\sqrt{c}}{1-c}$, $\chi_3 = \frac{2\pi}{r\kappa(r)} \frac{c\sqrt{c}}{1-c^3}$, and $\chi_5 = \frac{2\pi}{r\kappa(r)} \frac{c^2\sqrt{c}}{1-c^5}$, with $c = \exp[-\pi\kappa(\sqrt{1-r^2})/\kappa(r)]$ and $0 \leqslant r \leqslant 1$. Following Ndjomatchoua *et al.* [22,23], a Fourier expansion that approximates $u_0^{(2)}$ is

$$\frac{u_0^{(2)}(t)}{A} = \lambda_0 + \lambda_1 \cos(\omega t) + \lambda_2 \cos(2\omega t) + \lambda_3 \cos(3\omega t), \qquad (3)$$

where $\lambda_0 = r$, $\lambda_1 = 1 - r^2$, $\lambda_2 = -(1-r^2)r$, and $\lambda_3 = (1 - r^2)r^2$. This second approximation is more accurate for $|r| \leqslant 0.5$. The approximations in Eqs. (2) and (3) correctly match their original analog in Eq. (1). Since the coefficients χ_i, $i = 1, 3, 5$ and λ_i, $i = 1, 2, 3$, respectively, are of the same order, and considering the contribution of higher harmonic terms to the fundamental frequency's signal (ω), the solutions to the FPU lattice equation are sought in the form

$$u_n^{(1)}(t) = \frac{1}{2} A_n(t) \sum_{\ell=0}^{2} \chi_{2\ell+1} \exp[\jmath((2\ell+1)\omega t - qn)] + \text{c.c.},$$

$$u_n^{(2)}(t) = \lambda_0 A_n(t) + \frac{1}{2} A_n(t) \sum_{\ell=1}^{3} \lambda_\ell \exp[\jmath(\ell\omega t - qn)] + \text{c.c.},$$

where $\jmath^2 = -1$, and c.c. stands for the complex conjugate. In what follows, the triplets (χ_1, χ_3, χ_5) and $(\lambda_1, \lambda_2, \lambda_3)$ will be uniquely denoted $(\varrho_1, \varrho_2, \varrho_3)$. After inserting these *Ansätze* in the FPU equation, and consider the slowly varying envelope approximation (in space and time), we use the continuum approximation $[A_n(t) \to A(x,t)]$ and Taylor's expansion. We obtain at the edge $q = \pi$ of the first Brillouin zone, when collecting terms of $\exp(\jmath\omega t)$, the well-known nonlinear Schrödinger equation

$$-\jmath\partial_t A + \left(\frac{\omega^2 - 4}{2\omega}\right)A - \frac{1}{2\omega}\partial_x^2 A - Q|A|^2 A = 0,$$

$$Q = \frac{6}{\omega}\left(\varrho_1^2 + 2\varrho_2^2 + 2\varrho_3^2 + \frac{\varrho_2^2\varrho_3}{\varrho_1}\right), \qquad (4)$$

where $\partial_t \equiv \partial/\partial t$ and $\partial_x^2 \equiv \partial^2/\partial x^2$. Similarly to [8,27,29], the supratransmission threshold (A_{th}) is obtained through the maximum amplitude of the static breather solution of Eq. (4). Since this last equation is derived through terms of $\exp(\jmath\omega t)$, only terms of $\cos(\ell\omega t)$, $\ell \leqslant 1$ shall be considered for the derivation of the threshold, which is thus expressed as

$$A_{\text{th}}(\omega, r) = \gamma \sqrt{\frac{\omega^2 - 4}{6\varrho_1^2 + 12\varrho_2^2 + 12\varrho_3^2 + 6\frac{\varrho_2^2\varrho_3}{\varrho_1}}}, \qquad (5)$$

where $\gamma = \chi_1$ and $\gamma = |\lambda_0| + \lambda_1$ for symmetric $[u_0^{(1)}(t)]$ and asymmetric $[u_0^{(2)}(t)]$ shape signals, respectively, and $\varrho_i = \varrho_i(r)$, $i = 1, 2, 3$. When $r = 0$, we recover the NST threshold $A_{\text{th}} = \sqrt{(\omega^2 - 4)/6}$ previously found by Khomeriki *et al.* [27].

Energy Transmission Control. The nonlinear supratransmission allows energy to flow through the medium with the condition $\omega > 2$. Following the literature [14], the NST threshold is estimated numerically by the brute-force method combined with the dichotomic search with a precision of 10^{-6}. This energy flow below and above the threshold is studied with the energy density flux between two consecutive particles [20,27],

$$J_{n,n+1} = (\dot{u}_n - \dot{u}_{n-1})[(u_n - u_{n-1}) + (u_n - u_{n-1})^3]. \qquad (6)$$

The size of the lattice is fixed at $N = 100$ particles. To avoid initial shocks, the signal shall be introduced smoothly $(u_0(t) \to u_0[1 - \exp(-t/\tau)]$, with $\tau = 10)$ in the system, with the chain initially at rest $[u_n(0) = \dot{u}_n(0) = 0]$ [14,27]. The reflected waves coming back from the boundary $n = N$ are attenuated by adding a dissipative term $(-\gamma\dot{u}_n$, with $\gamma = 5)$ to the last ten particles [14,27]. The threshold [Eq. (5)] versus the driving frequency is plotted together with its numerical analog for the symmetric and asymmetric signals shape deformations (Fig. 2). A good agreement between both solutions can be observed. Moreover, displaying the energy density as a function of the shape parameter for fixed values of the driving amplitude illustrates the following:

(i) A sharp increase (revealing the NST triggering) for the case of symmetric shape deformation [Fig. 3(a)].

(ii) A sharp increase (NST triggering), followed by a zone of nonzero density (energy transmission), and thereafter a sharp decrease (suppression of NST) for the case of asymmetric shape deformation [Fig. 3(b)].

The NST threshold value $A = A_{\text{th}} = 1.229$, which was found early for a FPU lattice driven by a sinusoidal signal of frequency $\omega = 3.5$ [27], emerges distinctly ($J_{50,51} > 0$) for $r = 0$ [Fig. 3(c)]. Surprisingly, Fig. 3(a) reveals an energy

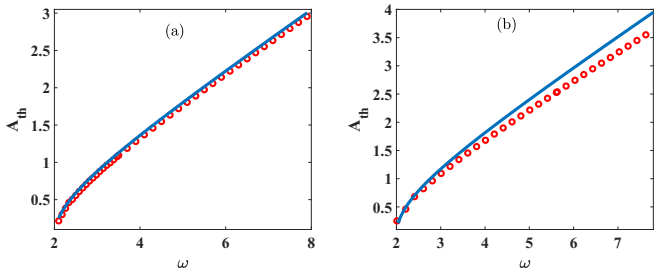

FIG. 2. Analytical (blue solid lines) and numerical (red circles) thresholds vs driving frequency for symmetric (a) and asymmetric (b) shape deformations; $r = 0.5$ (a) and $r = 0.99$ (b).

propagation for a driving amplitude $A = 1.1$ triggered at a critical shape parameter value $r = 0.984$ of the signal $u_0^{(1)}$. In contrast, when considering the signal $u_0^{(2)}$ with an amplitude of $A = 1.4$ [Fig. 3(b)], the wave transmission does not occur when the shape parameter is beyond $|r| = 0.35$. On the range of interesting observations, we note a decrease of the supratransmission threshold with the increase of the shape parameter in the case of symmetric shape deformation and, in contrast, an increase of this threshold with the increase of the absolute value of the shape parameter in the asymmetric case (Fig. 4), revealing that the supratransmission is strongly dependent on the shape of the periodic signal.

The difference in behavior between the two analyzed signals regarding the NST threshold is not due to symmetry but rather stems from the interaction among various harmonics observed in the Fourier series expansion. Specifically, for the symmetric signal, the coefficients of the harmonics are exclusively positive, leading to cooperative effects that amplify the amplitude of the fundamental harmonic up to that of the sinusoidal signal $A\sin(\omega t)$. This amplification boosts its energy,

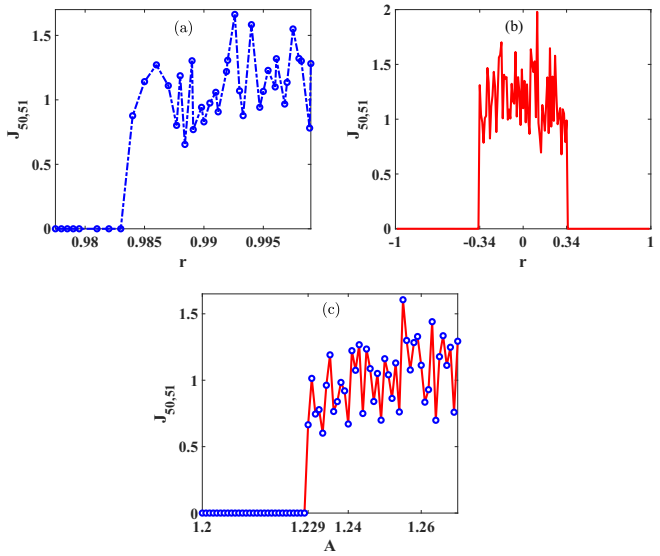

FIG. 3. Energy density flux at the middle of the nonlinear chain $J_{50,51}$ vs the shape parameter for symmetric deformation (a) and asymmetric deformation (b). Energy density vs the driving amplitude for shape parameter $r = 0$ (c). $A_0 = 1.1$ (a) and $A = 1.4$ (b). For all three subfigures, $\omega = 3.5$.

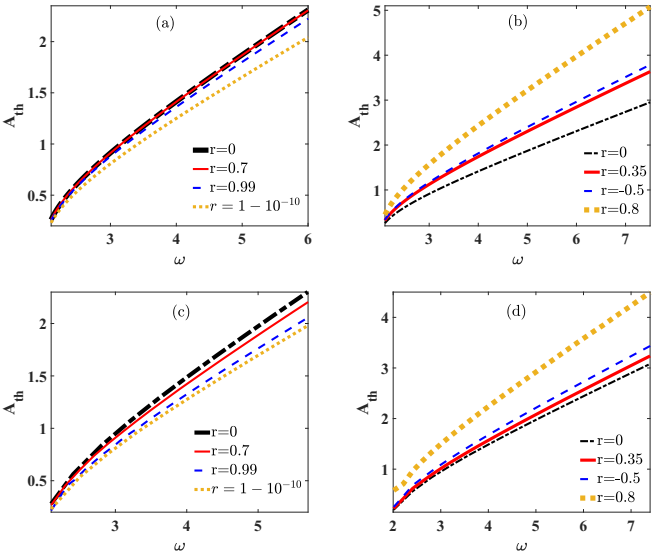

FIG. 4. Analytical (a),(b) and numerical (c),(d) threshold vs driving frequency in the FFBG for several values of r. (a) and (c) Symmetric, (b) and (d) asymmetric deformations.

subsequently resulting in the reduction of the NST threshold. Conversely, for the asymmetric signal, the coefficients of the harmonics can vary in sign, resulting in competitive effects that diminish the amplitude of the fundamental harmonic below A. Consequently, more energy is required to initiate supratransmission, thereby enhancing the NST threshold. This phenomenon can be visualized through the spectral representation of both external signals $u_0^{(1)}$ and $u_0^{(2)}$ (Fig. 5).

Discussion and Conclusion. Through this study on the supratransmission phenomenon with changing shape signals, we discovered that, contrary to popular belief, supratransmission is a phenomenon that depends on more than just the driving amplitude. The shape of the signal is an important parameter in the study of the phenomenon and should be considered in all studies on the subject.

Adjustment of the threshold, especially lowering it, is crucial in the quest for a purer waveform of solitonic pulses, as well as improving the efficiency and flexibility of hypersensitive detectors [32,33] and emitting solitonic pulses in a range of applications. The usage of defects can achieve an important threshold reduction [17]. Although they achieve a good result, such approaches cannot be easily implemented due to the need to modify the system itself at specific lattice

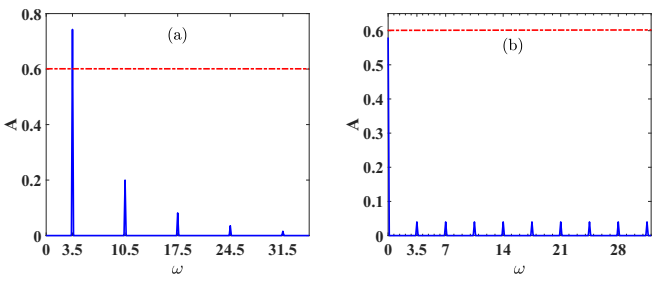

FIG. 5. Spectral density of the signals $u_0^{(1)}$ (a) and $u_0^{(2)}$ (b). $\omega = 3.5$, $A = 0.6$, $r = 0.9999$. Red dash-dotted lines stand for the driving amplitude values.

locations [17]. This study demonstrated that a well-selected shape for the exciting signal can achieve a satisfying result without modifying the system.

Other original methods were employed to transmit a periodic wave with an amplitude below the threshold. This wave can propagate if another harmonic driving is added at the right end [15], or if a noise is added in the initial incident driving [16]. The present study showed that the shape variation suffices to achieve wave energy flow in the lattice.

To experimentally verify the theoretical prediction of this work, such deformable signals may be easily built in a laboratory, for example using electrical circuits (e.g., see Ref. [22]).

In conclusion, the current research expands the nonlinear supratransmission notion by proving that an appropriate signal shape may induce (or block) energy flow through the lattice below (or above) the NST threshold, revealing that nonlinear supratransmission is dependent not only on driving amplitude but also on signal form, and thereafter that for a given frequency, there is not only one but rather an infinity of supratransmission thresholds depending on the shape of the driving signal.

[1] F. Geniet and J. Leon, Phys. Rev. Lett. **89**, 134102 (2002).
[2] K. T. V. Koon, P. Marquie, and P. T. Dinda, Phys. Rev. E **90**, 052901 (2014).
[3] H. Susanto, SIAM J. Appl. Math. **69**, 111 (2008).
[4] J. Leon, Phys. Lett. A **319**, 130 (2003).
[5] R. Khomeriki, Phys. Rev. Lett. **92**, 063905 (2004).
[6] P. Anghel-Vasilescu, J. Dorignac, F. Geniet, J. Leon, and M. Taki, Phys. Rev. Lett. **105**, 074101 (2010).
[7] J. E. Macías-Díaz, Phys. Rev. E **77**, 016602 (2008).
[8] C. Simadji Ngamou, F. T. Ndjomatchoua, M. Mekontchou Foudjio, C. L. Gninzalong, and C. Tchawoua, Phys. Rev. E **108**, 054216 (2023).
[9] M. Malishava and R. Khomeriki, Phys. Rev. Lett. **115**, 104301 (2015).
[10] A. B. Togueu Motcheyo and J. E. Macías-Díaz, Chaos Solitons Fractals **170**, 113349 (2023).
[11] J.-G. Cui, M.-Q. Niu, L.-Q. Chen, and T. Yang, Commun. Nonlin. Sci. Numer. Simul. **116**, 106885 (2023).
[12] H. Susanto, N. Lazarides, and I. Kourakis, Phys. Rev. E **108**, L052201 (2023).
[13] A. Bader and O. V. Gendelman, J. Sound Vib. **547**, 117493 (2023).
[14] M. Mekontchou Foudjio, F. Thomas Ndjomatchoua, C. Lawrence Gninzanlong, and C. Tchawoua, Chaos **30**, 123122 (2020).
[15] A. B. Togueu Motcheyo, C. Tchawoua, and J. D. Tchinang Tchameu, Phys. Rev. E **88**, 040901(R) (2013).
[16] S. B. Yamgoue, S. Morfu, and P. Marquie, Phys. Rev. E **75**, 036211 (2007).
[17] X. Liu, M. Wen, X. Mao, and X. Wang, Phys. Rev. E **104**, 014209 (2021).
[18] J. Lydon, G. Theocharis, and C. Daraio, Phys. Rev. E **91**, 023208 (2015).
[19] B. Yousefzadeh and A. S. Phani, J. Sound Vib. **380**, 242 (2016).
[20] M. Johansson, G. Kopidakis, S. Lepri, and S. Aubry, Europhys. Lett. **86**, 10009 (2009).
[21] T. Bountis, K. Kaloudis, J. Shena, C. Skokos, and C. Spitas, Eur. Phys. J. Spec. Top. **231**, 225 (2022).
[22] F. T. Ndjomatchoua, T. L. M. Djomo, F. F. Kemwoue, C. L. Gninzanlong, M. P. Kepnang, M. S. Siewe, C. Tchawoua, S. A. Pedro, and T. C. Kofane, Chaos **32**, 083144 (2022).
[23] F. T. Ndjomatchoua, C. L. Gninzanlong, T. L. M. Mbong Djomo, M. F. Pebeu Kepnang, and C. Tchawoua, Phys. Rev. E **107**, 064208 (2023).
[24] R. Chacón, P. J. Martínez, J. M. Marcos, F. J. Aranda, and J. A. Martínez, Phys. Rev. E **103**, 022203 (2021).
[25] J. Cuevas-Maraver, R. Chacón, and F. Palmero, Phys. Rev. E **94**, 062206 (2016).
[26] F. Palmero, J. Cuevas-Maraver, L. Q. English, W. Li, and R. Chacón, Phys. Scr. **94**, 065210 (2019).
[27] R. Khomeriki, S. Lepri, and S. Ruffo, Phys. Rev. E **70**, 066626 (2004).
[28] L. Brillouin, *Wave Propagation in Periodic Structures: Electronic Filters and Crystal Lattices* (McGraw-Hill, New York, 1946).
[29] A. B. Togueu Motcheyo and J. E. Macías-Díaz, J. Phys. A **53**, 505701 (2020).
[30] I. Kovacic, L. Cveticanin, M. Zukovic, and Z. Rakaric, J. Sound Vib. **380**, 1 (2016).
[31] A. Kiper, Math. Comp. **43**, 247 (1984).
[32] R. Khomeriki and J. Leon, Phys. Rev. Lett. **94**, 243902 (2005).
[33] D. Chevriaux, R. Khomeriki, and J. Leon, Phys. Rev. B **73**, 214516 (2006).